The Kinetic Alfvén-like nature of turbulent fluctuations in the Earth's magnetosheath: MMS measurement of the electron Alfvén ratio

O.W. Roberts,[1] Y. Narita,[1] R. Nakamura,[1] Z. Vörös,[1,2] and D. Verscharen[3]
[1)] *Space Research Institute, Austrian Academy of Sciences, Graz, 8010, Austria*
[2)] *Institute of Earth Physics and Space Science, Sopron, 9400, Hungary.*
[3)] *Mullard Space Science Laboratory, University College London, Dorking, RH5 6NT, UK*

(*Electronic mail: Owen.Roberts@oeaw.ac.at)

(Dated: 21 December 2021)

The Magnetospheric MultiScale (MMS) mission is used to investigate turbulent fluctuations in the Earth's magnetosheath. The unique combination of multiple spacecraft and high time resolution plasma and electromagnetic field data provided by MMS makes it an ideal mission to study the nature of turbulence and energy conversion. The multiple spacecraft allow the determination of the wavevector directions and plasma frame frequencies of the fluctuations. Moreover, the particle velocities allow the determination of the ion and electron Alfvén ratios, giving an additional diagnostic to reveal the nature of the turbulent fluctuations. Finally, the currents (determined from plasma moments) and the three-dimensional electric field measurements allow the determination of a scale-dependent energy conversion rate. The results reveal that the fluctuations predominantly have kinetic Alfvén wave-like properties at wavenumbers near $k\rho_i \sim 1$ (where ρ_i is the ion gyroradius) and that Landau damping is an important pathway for converting energy.

I. INTRODUCTION

Plasma turbulence is an ubiquitous process in the heliosphere. In-situ observations in the solar wind[1–3] and planetary magnetosheaths[4–8] reveal disordered fluctuations in electromagnetic fields and particle velocities. Energy is deposited into the system at large scales before undergoing a fluid-like turbulent cascade with eddies and fluctuations transferring energy to smaller scales. At the scales smaller than the particle gyration scales or where the particles decouple from the magnetic field, energy can be transferred efficiently from the fields to the particles' bulk kinetic and internal energies.

The exact mechanism or mechanisms behind plasma heating and acceleration in heliospheric plasma are unclear. Possible explanations include damping of electromagnetic waves[9–11] and dissipation in coherent structures[12,13]. Several different types of waves and coherent structures can exist in plasmas. At the moment, it is not clear how they interact with one another[14,15], and how they contribute to the observed heating and acceleration of particles. Identifying the nature of the fluctuations and comparing their polarization properties to those known from simplifying models (such as linear solutions to the Vlasov equation) can aid our understanding.

This paper aims to use both the multi-spacecraft capabilities of MMS and the high time resolution of particle data to understand the nature of the fluctuations in the Earth's magnetosheath and compare them to the predictions for waves from the linear Vlasov theory. The particle measurements of the current density $\mathbf{J}$ can also allow us to investigate $\mathbf{J}\cdot\mathbf{E}'$ (where $\mathbf{E}'$ denotes the electric field after transformation into a particle frame, i.e., ions or electrons) which quantifies the conversion of energy between the fields and the kinetic energy.

II. DATA/METHODOLOGY

On the 2^{nd} of September 2015, the MMS spacecraft[16] recorded an interval of Earth's magnetosheath in burst survey resolution. The spacecraft were located at [3.3,11.4,-0.2] Re in the GSE coordinate system (where X points from Earth to the Sun and Z points to the Solar ecliptic North). Magnetic field data were recorded from the fluxgate magnetometers[17] at a rate of 128 Hz. Plasma data were measured by the Fast Plasma Investigation[18] with a sampling rate of 6.6 Hz for ions and 30.3 Hz for electrons. Electric field data were recorded from the spin plane double probes (SDP)[19] which measure the x and y GSE components, and the axial double probe (ADP)[20] which measures the z component. Together, the SDP and ADP give a measurement of the three dimensional electric field with a sampling rate of 8.192 kHz. An overview of the data from the MMS1 spacecraft during the analyzed time interval presented in Fig 1.

The four MMS spacecraft make a regular tetrahedron with low values of planarity and elongation[21]; P=0.26 E=0.12 respectively and a mean inter-spacecraft distance of 140 km which is close to the ion's characteristic scales. This time interval occurred briefly after launch and was before MMS achieved its nominal separations of the order of tens of kilometers. The large formation is ideal for studying ion scale physics. The mean parameters (in GSE coordinates) are as follows: magnetic field B=[-15.2,24.0,41.1] nT, ion velocity [-214,154,-109] km/s, electron velocity [-195,144,-94] km/s. The measured ion density $n_i = 26.7$ cm^{-3} and electron density $n_e = 27.1$cm^{-3} are almost identical indicating a good quality of the measurements according to the constraint of quasi-neutrality. The ion Larmor radius and the inertial lengths are 43.3 km/rad and 43.7 km/rad, respectively, Ion and electron plasma parallel plasma β (the ratio of parallel thermal to magnetic pressure) are 0.61, 0.16 respectively.

To determine the wavevectors of the fluctuations in the plasma, we use two different, complementary meth-

ods. The first is the Multi-point signal resonator (MSR) technique[22] which is derived from wave-telescope/k-filtering methods[23,24]. This method assumes that the signal is weakly stationary and can be decomposed into a superposition of plane waves with a small component of incoherent noise. The main strength of this method is that multiple plane waves can be resolved at a single spacecraft frame frequency. The spatial scales accessible for investigation depend on the spacecraft separation with a Nyquist wavenumber of $k_{max} = \pi/\langle d \rangle$, where the angled brackets denote the average inter-spacecraft distance. We limit ourselves to a spacecraft frame frequency range between [0.1,1] Hz based on k_{max} and the ion bulk speed. The other method used is Bellan's method[25]; where the strength of this method is that only a single spacecraft is necessary. Bellan's method uses the measured magnetic field, and the plasma current density from the particle measurements $\mathbf{J}(t) = nq(\mathbf{V_i}(t) - \mathbf{V_e}(t))$ where the ion data are interpolated onto the electron time tags. Here n denotes the density (we use the electron density), q denotes the fundamental unit of charge,$\mathbf{V_i}$, and $\mathbf{V_e}$ denote the ion and electron velocities respectively. The wavevector is obtained following:

$$\mathbf{k}(\omega) = i\mu_0 \frac{\mathbf{J}(\omega) \times \mathbf{B}^*(\omega)}{\mathbf{B}(\omega) \cdot \mathbf{B}^*(\omega)} \tag{1}$$

Where the ω in the parentheses denotes that these are complex amplitudes from the Fourier transform. The asterisk denotes the complex conjugate. For this study we use the Bellan's method on each of the MMS spacecraft. Thus, the results presented are the mean of four independent measurements. Furthermore if one of the four wavevectors differ from the mean by an angle greater than 35° we eliminate these points from our analysis[26]. Bellan's method also assumes that the fluctuations can be described as a plane wave, and that there is only a single plane wave at each spacecraft frame freuqency such that each frequency maps to a single wavevector. No such assumption is necessary for the MSR technique, where multiple wavevectors can be detected at a single spacecraft frame frequency. However, we only investigate the wavevector with the largest power from the MSR method. Another difference is the range of wavenumbers that are accessible for investigation. The range of wavenumbers that can be resolved by the MSR method is set by the inter-spacecraft distances. Whereas for Bellan's method the limitation is from the length of the time series at large scales and the sampling rate/noise at small scales. The obtained wavevectors can then be used to obtain plasma frame frequencies according to the Doppler-shift relationship:

$$\omega_{pla} = \omega_{sc} - \mathbf{k} \cdot \langle \mathbf{V}_i \rangle. \tag{2}$$

The $\omega_{pla} - k$ relation can then be compared with linear solutions of the Vlasov equation.

III. RESULTS

Figure 2 shows the wavelet[27] power spectra of the trace magnetic field (using the Alfvén normalization to velocity units) (a), the trace electron velocity (b) the trace ion velocity (c) and the electron density (d). The vertical lines displayed on the spectra denote ion inertial length $d_i = V_A/\Omega_{ci}$, the ion gyroradius $\rho_i = v_{i\perp}/\Omega_{ci}$ and the combined scale $\rho_i + d_i$[28] which are expressed as Taylor shifted scale e.g. $f_{d_i} = V_{\rm bulk}/2\pi d_i$. The estimated noise floor of the measured quantities is also displayed along with the noise floor value multiplied by three for the ion velocity, the electron velocity and the electron density. For the magnetic field, the noise floor is outside the plotting range; the other quantities of noise floors are determined from the statistical errors of the measurements given in the level 2 moments data on the MMS data archive. The errors are used to define a white noise signal, e.g., Gershman et al. 2018[26]. A maximum reliable frequency is defined here as the frequency where the measured value is equal to three times the estimated noise floor[29].

At large scales above the Taylor shifted proton scales, it is difficult to determine the spectral index accurately as the interval is short and the cone of influence (COI) affects the results at large scales[27]. Consequently, there is only a limited range available to estimate the spectral index. We fit from a minimum value of 0.1 Hz (to limit the influence of the COI) up to the combined scale $f \sim 0.5$ Hz. At the smaller scales, we fit from the shifted ion inertial length scale to the maximum frequency $f_{\rm Max}$, where $f_{\rm Max}$ is different for each measurement. We choose these limits to avoid fitting over any of the relevant spatial scales. Furthermore, we avoid noise at small scales and the cone of influence at large scales. The black line indicated as f_B denotes the intersection of the two power-law fits. The magnetic field spectrum shows a typical steepening near the ion scales to an index near ~ -2.6 fairly typical in the solar wind and the magnetosheath[6,7,30–33]. At large scales $f < 0.2$ Hz the ion and electron velocity spectra are similar. At these scales, both ions and electrons are magnetized and thus coupled in their motion. At smaller scales the ion and electron velocity spectra begin to differ. The ion velocity spectra are much steeper at small scales ~ -3.3[6,34,35]. This is expected at these scales as the plasma leaves the MHD regime and ion-resonant dissipation sets in. The electron velocity spectrum is shallower than the ion velocity spectrum, and no clear break is observed. The density spectrum shows a similar slope to the magnetic spectrum at small scales, while at large scales, it is flatter. A flatter spectrum is often observed in the density in the solar wind forming a transition between the ion inertial and kinetic ranges and is sensitive to the β value[36–39]. However, our time series' are not long enough to compare larger scales to confirm that this is indeed a flattening.

The predictions from linear theory for the kinetic Alfvén wave[10,40–43] and the ion Bernstein wave[44] are calculated from the New Hampshire Dispersion Solver[45] using the mean parameters from the interval (plasma β, temperature anisotropy). The results are displayed in Fig 3, column 1, for the Alfvén branch, and column 2 for the Ion Bernstein branch. The propagation directions used are $\theta_{kb} = 80°$ (dashed lines)

and $\theta_{kb} = 89^\circ$ (solid lines), which is motivated from the typical wavevector anisotropy $k_\perp \gg k_\parallel$ often observed in plasma turbulence[46–48] and the wavevector observations from the interval (which will be discussed later). Fig 3 (a,b) shows the real frequencies in black and the imaginary part of the frequency in red (i.e. the damping rate). The KAW branch has low frequencies, while the ion Bernstein branch has much higher frequencies. However, we cannot distinguish between a quasi-perpendicular KAW and an advected structure (i.e., a spatial variation with $\omega_{pla} = 0$) using this methodology. The ambiguity comes from the uncertainty[48] and the natural fluctuations in the velocity[49] used for the Doppler shift (Eq. 2). Panel (c) displays the plasma frame frequency as a function of the wavenumber. The wavevector is determined from the MSR technique (blue) and Bellan's method (red). We apply the methods in the frequency range of 0.1- 1 Hz in the spacecraft frame. This frequency range corresponds to the Nyquist wavenumber set by the mean inter-spacecraft distance. The spacecraft frame frequency is obtained according to Eq 2. The obtained wavevectors make a quasi-perpendicular angle with the mean magnetic field direction $88 \pm 5^\circ$ from the MSR method and $82 \pm 15^\circ$ from Bellan's method (which justifies the propagation angles of the linear theory solutions). Bellan's method is applied to all four spacecraft and any wavevector which differs by an angle larger than 35° from the mean of all four is removed. Both methods produce consistent results, and fluctuations have low plasma frame frequencies compared to the cyclotron frequency except for one outlier in Bellan's method. The high frequency of this data point is likely due to more than one wavevector being present for a given Fourier mode which causes a large error in the Bellan method. However, the MSR method does not share this limitation and multiple wavevectors can be identified at a single frequency.

The second row denotes the ion (black) and electron (green) Alfvén ratios, which is the ratio of the trace velocity fluctuations to the trace magnetic fluctuations (in Alfvén units). The Alfvén ratio of species j is given by

$$R_{A,j} = \mu_0 n m_i \frac{\left|\delta \mathbf{v}_j\right|^2}{|\delta \mathbf{B}|^2}. \tag{3}$$

For the observations in panel (f), these are converted to a wavenumber following Taylor's hypothesis for the spacecraft measurements (other than the plasma frame frequency). It is important to recall that converting to a wavenumber this way does not give the true wavenumber of the fluctuations; instead, it gives a streamwise wavenumber denoted $k_{stream} = 2\pi f / V_i$. Where the streamwise wavenumber is related to $k_\perp$ as $k_{stream} = k_\perp \sin(\theta_{BV})\cos(\phi)$, where ϕ is the angle between $\mathbf{k}$ and the $\mathbf{B}$ $\mathbf{V}$ plane. If anisotropy $k_\perp \gg k_\parallel$ is assumed (which is observed for this interval), then $k_\perp \simeq k$ and ϕ is small then it follows that $k_{stream} \simeq k \sin(\theta_{BV})$.[50]. As $\theta_{BV} \simeq 80^\circ$ the difference between k and k_{stream} is expected to be small. The prediction of the Alfvén ratio for large-scale Alfvén waves, is 1, while for magnetosonic waves it is ~ 2 e.g. Gary (1986)[51]. For KAWs (panel d), near the ion gyro-length $k\rho_i \sim 1$ the ion and electron ratios begin to depart from one another. The magnetic field fluctuations' power become dominant over the ion velocity, while the electron velocity fluctuations' power becomes dominant. For the IBW (panel e), both ion and electron velocities are dominant. The observations in panel f which show a decrease in the ion Alfvén ratio with increasing wavenumber and an increase in the electron Alfvén ratio, which is more consistent with the predictions for kinetic Alfvén waves.

Row three denotes the cross-correlation between the magnitude of the magnetic field and the density for species j which is given by

$$CC = \frac{\Re(\delta n_j \delta |B|^*)}{|\delta n_j||\delta |B||}. \tag{4}$$

Where the asterisk denotes the complex conjugate. The Alfvén solutions and the IBW solutions show anti-correlated and correlated fluctuations respectively. The measurements show that the fluctuations are mostly anti-correlated throughout the ranges investigated, more consistent with the KAWs rather than the IBWs. In the final row, we see the magnetic compressibility defined as the fluctuations of the parallel component over the trace component,

$$C_B = \frac{|\delta B_\parallel|^2}{|\delta B_\parallel|^2 + |\delta B_{\perp 1}|^2 + |\delta B_{\perp 2}|^2}. \tag{5}$$

Where the parallel component is defined as the component along the mean magnetic field direction calculated over the interval. Throughout the range, they have a value of roughly 0.3, again more consistent with the KAW solutions rather than the IBW.

To understand the potential mechanisms for dissipation, we calculate the resonance parameters following[52,53]. For a species s, the resonance condition is quantifiable by:

$$\zeta = \frac{\omega_{pla} - m\Omega_s}{k_\parallel v_{s,thermal}} \tag{6}$$

where Ω_s is the cyclotron frequency of species s and $v_{s,thermal}$ is the thermal speed of species s, m is an integer with $m = 0$ giving the condition for Landau resonance and $m = \pm 1$ giving the condition for the first cyclotron resonance, the parameters k and ω_{pla} are determined from the MSR, and Bellan's method, presented in Fig 3a. When $\zeta \approx 1$, then resonant energy transfer from the electromagnetic fields can occur efficiently. We note that our definition of ζ in Eq. 6 is based on the thermal speed, while the full velocity distribution of the particles provide an infinite range of velocities that can potentially resonate. Nevertheless, the thermal speed is appropriate for characterizing a significant number of particles that can efficiently resonate[54]. The mean values of the resonance parameters are presented in Tab I. Both methods have consistent results and suggest that the ion and Landau resonances may be possible in the interval; however, for cyclotron resonance, $\zeta \gg 1$ for both ions and electrons[52,53]. For ion scales we do not expect the electron cyclotron resonance to

TABLE I. The mean, the standard deviations and the min/max values of the resonance parameter analysis

	Mean	Standard Deviation	Min	Max
Ion Landau (MSR)	3.6	3.9	0.18	14.85
Electron Landau (MSR)	0.2	0.2	0.01	0.84
Ion Landau (Bellan)	3.7	3.9	0.19	13.44
Electron Landau (Bellan)	0.2	0.2	0.01	0.76
Ion Cyclotron (MSR)	97	159	10	600
Electron Cyclotron (MSR)	10000	16000	900	60000
Ion Cyclotron (Bellan)	17	15	2	50
Electron Cyclotron (Bellan)	1400	1300	100	4000

be active, this is reflected in the result that the resonance parameters are much larger than 1. Should we measure larger wavevectors which is possible for the smaller MMS separations, perhaps the electron cyclotron resonance becomes more important. The standard deviations are large for all cases. The large standard deviations are due to the difficulty in measuring the parallel wavenumber, which is small and can cause the resonance parameter to become very large as it is in the denominator of Eq. 6.

Figure 4 shows the evolution of the resonance parameters as a function of the wavenumber. The error bars denote the relative error of the resonance parameters. Note that some of the errors are large as the frequency measured is low in some cases which leads to a large relative error despite the absolute error being small. The dashed line indicates a resonance parameter of 1. Even considering the error bars, the resonance condition for either cyclotron resonance is not fulfilled. For the ion Landau resonance, the points are predominantly above 1 but some errors straddle and some points lie beneath the value of unity, indicating that ion Landau resonance could be occurring. For the electron Landau resonance, the points are all below 1 but in general, show a trend towards 1. At smaller scales than studied here ($k\rho_i > 1.6$) it is possible that electron Landau damping becomes more important. Observations of magnetic spectra show steepening at roughly $5 > k\rho_i > 30$[31,32,46,55,56] which could be interpreted as being due to the onset of electron Landau damping[57].

To further investigate Landau damping as a potential mechanism for the conversion of energy from the fields to the kinetic energies, we investigate $\mathbf{J}\cdot\mathbf{E}'$[58]. Note that electric fields are frame dependent, so the measured spacecraft frame electric field needs to be transformed to the rest frame[59,60] using a mean measured velocity $\mathbf{E}' = \mathbf{E} + \langle \mathbf{V}_i \rangle \times \mathbf{B}$ (i.e., subtracting the convective electric field). Here the mean ion bulk velocity vector is used, although, both the mean electron and ion bulk flows are similar in this interval. The $\mathbf{J}\cdot\mathbf{E}'$ parameter is the work done on the particles by the electric field and quantifies the transfer of energy between the fields and the particle kinetic energy. This is not strictly speaking dissipation as the energy is transferred to the kinetic energy rather than the internal energy of the particles[61–63].

To obtain a scale dependent measure of the energy conversion we use an energy conversion rate[64,65] defined as;

$$\varepsilon_{ECR} = \frac{1}{4}(\tilde{\mathbf{J}}\cdot\tilde{\mathbf{E}}'^{*} + \tilde{\mathbf{J}}^{*}\cdot\tilde{\mathbf{E}}') \tag{7}$$

where the tildes denote the wavelet coefficients of $\mathbf{J}$ and $\mathbf{E}'$ and the asterisk denotes the complex conjugate. The scale-dependent ε_{ECR} is shown for the perpendicular direction, and the parallel direction in Fig 5 where the dashed lines denote the mean value, and the shaded region denotes the standard deviation. The energy conversion rate in the parallel direction is defined as;

$$\varepsilon_{ECR,\parallel} = \frac{1}{4}(\tilde{J_\parallel}\cdot\tilde{E_\parallel'}^{*} + \tilde{J_\parallel}^{*}\cdot\tilde{E_\parallel'}) \tag{8}$$

while in the perpendicular direction it is defined as;

$$\varepsilon_{ECR,\perp} = \frac{1}{4}\left[(\tilde{J_{\perp 1}}\cdot\tilde{E_{\perp 1}'}^{*} + \tilde{J_{\perp 1}}^{*}\cdot\tilde{E_{\perp 1}'}) + (\tilde{J_{\perp 2}}\cdot\tilde{E_{\perp 2}'}^{*} + \tilde{J_{\perp 2}}^{*}\cdot\tilde{E_{\perp 2}'})\right] \tag{9}$$

At large scales Fig 5a $k\rho_i < 0.5$ there is a significant fluctuation in the perpendicular value of the energy conversion rate whereas the parallel component is close to zero (Fig5b). The large variations in the perpendicular energy conversion rate are associated with large-scale velocity fluctuations, e.g., those at 14:57:40-14:58:00 (see Fig1).

To get a clearer view of the fluctuations near $k\rho_i \sim 1$ we re-plot figures 5a,b, only between $k\rho_i = 0.5-7$ with a limited y-axis. Figure 5d shows that the parallel component of the energy conversion rate is positive, which is suggestive of Landau damping. The standard deviations are large, indicating a transfer of energy in both directions; however, the secular net transfer is from the fields to the particles. The mean value is close to zero in the perpendicular components but is negative at the larger scales.

IV. DISCUSSION

The nature of the ion and electron Alfvén ratios shows a good match with the expectations from linear Vlasov theory for a KAW. Consistent with the observations of Roberts et al (2018)[66] for the ion Alfvén ratio. We rule out the kinetic slow mode as its ion Alfvén ratio increases with increasing wavenumber[67]. The cross-correlations of density and magnetic field magnitude are also consistent with the KAW interpretation, as IBWs have the same positive correlations as MHD scale fast waves. Finally, the measured compressibility also matches the expectation for KAWs well. Kinetic slow waves and IBWs are expected to have $C_B \sim 1$. At scales $k\rho_i < 0.5$, the compressibility is larger than predicted for a KAW. The large compressibility is most likely due to fluid scale compressive coherent structures which have anti-correlated $n_e - B$ and similar Alfvénicities to KAWs but are more compressive. Possible structures could be compressive vortices e.g.[68] magnetic holes/mirror modes[69], pressure balanced structures[70,71]. Kinetic slow waves could also contribute; however, they are typically strongly damped, although

the low β in this interval may allow them to exist longer than in high-β intervals.

While we interpret the results by comparing them with linear wave solutions, it is possible that the fluctuations are not wave-like. After numerous wave-wave interactions due to the turbulent cascade, the frequency of a wave can be broadened[72,73] to be sideband waves[74,75] which do not necessarily correspond to a single wave as predicted from Vlasov theory[76,77]. Another possible wave interaction is the parametric instability[10,41,78] that can occur whenever the Alfvén wave interacts with a background density fluctuation. Even though the fluctuation level is ($\delta B/B_0 = 0.15$) in our study, parametric instabilities are plausible explanations to the observed data. Theoretical and numerical studies indicate that cross scale coupling[79] can occur and some of the daughter waves can propagate nearly perpendicular to the mean magnetic field[78,80,81]. The existence of three-wave couplings acting on the ion Bernstein waves is also indicated by the numerical study by[82].

The results do suggest that Landau resonances of the ions and the electrons are more important than the cyclotron resonances consistent with the expectations of a kinetic Alfvén wave[10,40,42] and with a field-particle analysis of electrons carried out by Chen et al (2019)[11] on a different magnetosheath interval. We note that the standard deviations of the resonance parameters is large, however considering the range of values the Landau resonances are likely more important than the cyclotron resonances in this interval. Further evidence of the importance of electron Landau damping comes from a wave-driven simulation of TenBarge et al. (2013)[83] which finds that heating in current sheets through the Landau resonance is more likely than Ohmic dissipation (due to the low collisionality).

Our results also suggest that ion Landau damping may be possible at these scales and electron Landau damping at smaller scales. A short variable 'transition range' is often observed in the solar magnetic field power spectrum between the inertial and the dissipation scales.[3,46,84]. This has been interpreted as being due to ion Landau damping[46]. Although the resonance parameters are not equal to 1, the linear theory damping rates suggest that we are at slightly larger scales than where we expect damping to occur for a linear KAW. Investigation of the parallel energy conversion rate also suggests Landau damping is present at $k\rho_i > 0.5$.

To better understand the dissipation processes at various scales, numerous intervals should be analyzed with spacecraft separations near the different plasma scale lengths. It would be preferable to perform this with the same interval with multiple spacecraft[85,86]. Such a study is possible with multiple data intervals from the Cluster spacecraft or the MMS spacecraft. However, for MMS, the range of separations is relatively small, leading to a small number of time intervals with ion-scale separations.

V. CONCLUSION

We have used the unique properties of MMS to reveal the properties of fluctuations near the ion kinetic scales in magnetosheath turbulence. The multiple spacecraft and the ability to measure the plasma current at high time resolutions enable the determination of the wavevector with two different approaches. The fluctuations at these scales have low plasma frame frequencies consistent with KAWs or advected structures that have no intrinsic frequency.

Other properties such as the ion and electron Alfvén ratios, cross-correlations between the compressive magnetic field and magnetic compressibility agree well with the linear theory predictions for KAWs. However, as turbulence is an inherently nonlinear process, it is not apparent that these are signatures of waves in the classical sense. At larger scales ($k\rho_i \sim 0.1$), the compressibility is too large to be explained in terms of linear KAWs. Furthermore, there is energy transfer occurring in this range which is associated with regions with large scale fluctuations. Therefore while the KAW interpretation is consistent with the results, it does not seem to be a complete description.

Finally, we remark that the measured resonance parameters suggest that in this interval at these scales, cyclotron resonance either with electrons or ions is not important. The resonance parameters and $\mathbf{J}\cdot\mathbf{E}'$ support that Landau resonance is important for the conversion of energy from the fields to kinetic energy in the magnetosheath.

ACKNOWLEDGMENTS

R.N. was supported by Austrian FWF Project No. I2016-N20. Z.V. was supported by the Austrian FWF Project No. P28764-N27. D.V. is supported by STFC Ernest Rutherford Fellowship ST/P003826/1 and STFC Consolidated Grant ST/S000240/1.

DATA AVAILABILITY STATEMENT

The data that support the findings of this study are openly available in the MMS data archive, `https://lasp.colorado.edu/mms/sdc/public/`,[87]

[1] C. Y. Tu and E. Marsch, "MHD structures, waves and turbulence in the solar wind: Observations and theories," Space Science Reviews **73**, 1–210 (1995).
[2] R. Bruno and V. Carbone, "The Solar Wind as a Turbulence Laboratory," Living Reviews in Solar Physics **10** (2013), 10.12942/lrsp-2013-2.
[3] O. Alexandrova, C. H. K. Chen, L. Sorriso-Valvo, T. S. Horbury, and S. D. Bale, "Solar Wind Turbulence and the Role of Ion Instabilities," in *Space Science Reviews*, Vol. 178 (2013) pp. 25–63.
[4] O. Alexandrova, "Solar wind vs magnetosheath turbulence and Alfvén vortices," Nonlinear Processes in Geophysics **15**, 95–108 (2008).
[5] O. Alexandrova and J. Saur, "Alfvén vortices in Saturn's magnetosheath: Cassini observations," Geophysical Research Letters **35**, L15102 (2008).
[6] C. H. K. Chen and S. Boldyrev, "Nature of Kinetic Scale Turbulence in the Earth's Magnetosheath," The Astrophysical Journal **842**, 122 (2017), arXiv:1705.08558.

[7]L. Matteini, O. Alexandrova, C. H. K. Chen, and C. Lacombe, "Electric and magnetic spectra from MHD to electron scales in the magnetosheath," Monthly Notices of the Royal Astronomical Society **466**, 945–951 (2017).
[8]O. W. Roberts, Y. Narita, R. Nakamura, Z. Vörös, and D. Gershman, "Anisotropy of the Spectral Index in Ion Scale Compressible Turbulence: MMS Observations in the Magnetosheath," Frontiers in Physics **7**, 1–16 (2019).
[9]R. J. Stefant, "Alfven Wave Damping from Finite Gyroradius Coupling to the Ion Acoustic Mode," Physics of Fluids **13**, 440 (1970).
[10]A. Hasegawa and L. Chen, "Kinetic process of plasma heating due to Alfvén wave excitation," Physical Review Letters **35** (1975).
[11]C. H. K. Chen, K. G. Klein, and G. G. Howes, "Evidence for electron Landau damping in space plasma turbulence," Nature Communications **10** (2019), 10.1038/s41467-019-08435-3.
[12]K. Osman, W. Matthaeus, A. Greco, and S. Servidio, "Evidence for Inhomogeneous Heating in the Solar Wind," The Astrophysical Journal **727**, L11 (2011).
[13]R. Bandyopadhyay, A. Chasapis, R. Chhiber, T. N. Parashar, W. H. Matthaeus, M. A. Shay, B. A. Maruca, J. L. Burch, T. E. Moore, C. J. Pollock, B. L. Giles, W. R. Paterson, J. Dorelli, D. J. Gershman, R. B. Torbert, C. T. Russell, and R. J. Strangeway, "Incompressive Energy Transfer in the Earth's Magnetosheath: Magnetospheric Multiscale Observations," The Astrophysical Journal **866**, 106 (2018), arXiv:1806.04275.
[14]D. Grošelj, C. H. K. Chen, A. Mallet, R. Samtaney, K. Schneider, and F. Jenko, "Kinetic Turbulence in Astrophysical Plasmas: Waves and/or Structures?" Physical Review X **9**, 031037 (2019), arXiv:1806.05741.
[15]O. W. Roberts, D. Verscharen, Y. Narita, R. Nakamura, Z. Vörös, and F. Plaschke, "Possible coexistence of kinetic Alfvén and ion Bernstein modes in sub-ion scale compressive turbulence in the solar wind," Physical Review Research **2**, 43253 (2020).
[16]J. L. Burch, T. E. Moore, R. B. Torbert, and B. L. Giles, "Magnetospheric Multiscale Overview and Science Objectives," Space Science Reviews **199**, 5–21 (2016).
[17]C. T. Russell, B. J. Anderson, W. Baumjohann, K. R. Bromund, D. Dearborn, D. Fischer, G. Le, H. K. Leinweber, D. Leneman, W. Magnes, J. D. Means, M. B. Moldwin, R. Nakamura, D. Pierce, F. Plaschke, K. M. Rowe, J. A. Slavin, R. J. Strangeway, R. Torbert, C. Hagen, I. Jernej, A. Valavanoglou, and I. Richter, "The Magnetospheric Multiscale Magnetometers," Space Science Reviews **199**, 189–256 (2016).
[18]C. Pollock, T. Moore, A. Jacques, J. Burch, U. Gliese, Y. Saito, T. Omoto, L. Avanov, A. Barrie, V. Coffey, J. Dorelli, D. Gershman, B. Giles, T. Rosnack, C. Salo, S. Yokota, M. Adrian, C. Aoustin, C. Auletti, S. Aung, V. Bigio, N. Cao, M. Chandler, D. Chornay, K. Christian, G. Clark, G. Collinson, T. Corris, A. De Los Santos, R. Devlin, T. Diaz, T. Dickerson, C. Dickson, A. Diekmann, F. Diggs, C. Duncan, A. Figueroa-Vinas, C. Firman, M. Freeman, N. Galassi, K. Garcia, G. Goodhart, D. Guererro, J. Hageman, J. Hanley, E. Hemminger, M. Holland, M. Hutchins, T. James, W. Jones, S. Kreisler, J. Kujawski, V. Lavu, J. Lobell, E. LeCompte, A. Lukemire, E. MacDonald, A. Mariano, T. Mukai, K. Narayanan, Q. Nguyan, M. Onizuka, W. Paterson, S. Persyn, B. Piepgrass, F. Cheney, A. Rager, T. Raghuram, A. Ramil, L. Reichenthal, H. Rodriguez, J. Rouzaud, A. Rucker, Y. Saito, M. Samara, J.-A. Sauvaud, D. Schuster, M. Shappirio, K. Shelton, D. Sher, D. Smith, K. Smith, S. Smith, D. Steinfeld, R. Szymkiewicz, K. Tanimoto, J. Taylor, C. Tucker, K. Tull, A. Uhl, J. Vloet, P. Walpole, S. Weidner, D. White, G. Winkert, P.-S. Yeh, and M. Zeuch, "Fast Plasma Investigation for Magnetospheric Multiscale," Space Science Reviews **199**, 331–406 (2016).
[19]P.-A. Lindqvist, G. Olsson, R. B. Torbert, B. King, M. Granoff, D. Rau, G. Needell, S. Turco, I. Dors, P. Beckman, J. Macri, C. Frost, J. Salwen, A. Eriksson, L. Åhlén, Y. V. Khotyaintsev, J. Porter, K. Lappalainen, R. E. Ergun, W. Wermeer, and S. Tucker, "The Spin-Plane Double Probe Electric Field Instrument for MMS," Space Science Reviews **199**, 137–165 (2016).
[20]R. E. Ergun, S. Tucker, J. Westfall, K. A. Goodrich, D. M. Malaspina, D. Summers, J. Wallace, M. Karlsson, J. Mack, N. Brennan, B. Pyke, P. Withnell, R. Torbert, J. Macri, D. Rau, I. Dors, J. Needell, P. A. Lindqvist, G. Olsson, and C. M. Cully, "The Axial Double Probe and Fields Signal Processing for the MMS Mission," Space Science Reviews **199**, 167–188 (2016).
[21]P. Robert, A. Roux, C. Harvey, M. Dunlop, P. Daly, and K.-H. Glassmeier, "Tetrahedron Geometric Factors," in *Analysis Methods for Multi-Spacecraft Data*, edited by P. Paschmann, G Daly (1998) Chap. 13, pp. 323–348.
[22]Y. Narita, K.-H. Glassmeier, and U. Motschmann, "High-resolution wave number spectrum using multi-point measurements in space – the Multi-point Signal Resonator (MSR) technique," Annales Geophysicae **29**, 351–360 (2011).
[23]J. Pincon and F. Lefeuvre, "Local characterization of homogeneous turbulence in a space plasma from simultaneous measurements of field components at several points in space," Journal of Geophysical Research **96**, 1789–1802 (1991).
[24]U. Motschmann, T. I. Woodward, K. H. Glassmeier, D. J. Southwood, and J. L. Pinçon, "Wavelength and direction filtering by magnetic measurements at satellite arrays: Generalized minimum variance analysis," Journal of Geophysical Research: Space Physics **101**, 4961–4965 (1996).
[25]P. M. Bellan, "Revised single-spacecraft method for determining wave vector k and resolving space-time ambiguity," Journal of Geophysical Research A: Space Physics **121**, 8589–8599 (2016).
[26]D. J. Gershman, A. F.-Viñas, J. C. Dorelli, M. L. Goldstein, J. Shuster, L. A. Avanov, S. A. Boardsen, J. E. Stawarz, S. J. Schwartz, C. Schiff, B. Lavraud, Y. Saito, W. R. Paterson, B. L. Giles, C. J. Pollock, R. J. Strangeway, C. T. Russell, R. B. Torbert, T. E. Moore, and J. L. Burch, "Energy partitioning constraints at kinetic scales in low- β turbulence," Physics of Plasmas **25**, 022303 (2018).
[27]C. Torrence and G. P. Compo, "A Practical Guide to Wavelet Analysis," Bulletin of the American Meteorological Society **79**, 61–78 (1998).
[28]R. Bruno and L. Trenchi, "RADIAL DEPENDENCE OF THE FREQUENCY BREAK BETWEEN FLUID AND KINETIC SCALES IN THE SOLAR WIND FLUCTUATIONS," The Astrophysical Journal **787**, L24 (2014).
[29]O. Alexandrova, J. Saur, C. Lacombe, A. Mangeney, S. J. Schwartz, J. Mitchell, R. Grappin, P. Robert, M. Maksimovic, K. Issautier, N. Meyer-Vernet, M. Moncuquet, and F. Pantellini, "Solar wind turbulent spectrum from MHD to electron scales," in *AIP Conference Proceedings*, Vol. 1216 (2010) pp. 144–147.
[30]C. W. Smith, K. Hamilton, B. J. Vasquez, and R. J. Leamon, "Dependence of the Dissipation Range Spectrum of Interplanetary Magnetic Fluctuationson the Rate of Energy Cascade," The Astrophysical Journal **645**, L85–L88 (2006).
[31]O. Alexandrova, J. Saur, C. Lacombe, A. Mangeney, J. Mitchell, S. Schwartz, and P. Robert, "Universality of Solar-Wind Turbulent Spectrum from MHD to Electron Scales," Physical Review Letters **103** (2009), 10.1103/PhysRevLett.103.165003.
[32]O. Alexandrova, C. Lacombe, A. Mangeney, R. Grappin, and M. Maksimovic, "Solar Wind Turbulent Spectrum At Plasma Kinetic Scales," The Astrophysical Journal **760**, 121 (2012).
[33]S. Y. Huang, F. Sahraoui, X. H. Deng, J. S. He, Z. G. Yuan, M. Zhou, Y. Pang, and H. S. Fu, "KINETIC TURBULENCE IN THE TERRESTRIAL MAGNETOSHEATH: CLUSTER OBSERVATIONS," The Astrophysical Journal **789**, L28 (2014), arXiv:1312.5167.
[34]J. E. Stawarz, S. Eriksson, F. D. Wilder, R. E. Ergun, S. J. Schwartz, A. Pouquet, J. L. Burch, B. L. Giles, Y. Khotyaintsev, O. L. Contel, P. A. Lindqvist, W. Magnes, C. J. Pollock, C. T. Russell, R. J. Strangeway, R. B. Torbert, L. A. Avanov, J. C. Dorelli, J. P. Eastwood, D. J. Gershman, K. A. Goodrich, D. M. Malaspina, G. T. Marklund, L. Mirioni, and A. P. Sturner, "Observations of turbulence in a Kelvin-Helmholtz event on 8 September 2015 by the Magnetospheric Multiscale mission," Journal of Geophysical Research: Space Physics **121**, 11,021–11,034 (2016).
[35]O. W. Roberts, S. Toledo-Redondo, D. Perrone, J. Zhao, Y. Narita, D. Gershman, R. Nakamura, B. Lavraud, C. P. Escoubet, B. Giles, J. Dorelli, C. Pollock, and J. Burch, "Ion-Scale Kinetic Alfvén Turbulence: MMS Measurements of the Alfvén Ratio in the Magnetosheath," Geophysical Research Letters **45**, 7974–7984 (2018).
[36]B. D. G. Chandran, E. Quataert, G. G. Howes, Q. Xia, and P. Pongkitiwanichakul, "Constraining Low-Frequency Alfvenic Turbulence in the Solar Wind using Density-Fluctuation Measurements," The Astrophysical Journal **707**, 1668–1675 (2009).
[37]C. H. K. Chen, G. G. Howes, J. W. Bonnell, F. S. Mozer, K. G. Klein, and S. Bale, "Kinetic Scale Density Fluctuations in the Solar Wind," in *Solar Wind 13* (2012) pp. 1–5, arXiv:1210.0127v1.
[38]O. W. Roberts, R. Nakamura, K. Torkar, Y. Narita, J. C. Holmes, Z. Vörös, C. Lhotka, C. P. Escoubet, D. B. Graham, D. J. Gershman, Y. Khotyaintsev,

and P.-A. Lindqvist, "Sub-ion Scale Compressive Turbulence in the Solar Wind: MMS Spacecraft Potential Observations," The Astrophysical Journal Supplement Series **250**, 35 (2020).

[39] O. W. Roberts, J. Thwaites, L. Sorriso-Valvo, R. Nakamura, and Z. Vörös, "Higher-Order Statistics in Compressive Solar Wind Plasma Turbulence: High-Resolution Density Observations From the Magnetospheric Multi-Scale Mission," Frontiers in Physics **8**, 1–14 (2020).

[40] L. Chen and A. Hasegawa, "Plasma heating by spatial resonance of Alfvén wave," Physics of Fluids , 1399–1403 (1974).

[41] A. Hasegawa and L. Chen, "Kinetic processes in plasma heating by resonant mode conversion of Alfven wave," Physics of Fluids **19**, 1924 (1976).

[42] J. Hollweg, "Kinetic Alfvén wave revisited," Journal of geophysical research **104**, 811–819 (1999).

[43] Y. Narita, O. W. Roberts, Z. Vörös, and M. Hoshino, "Transport Ratios of the Kinetic Alfvén Mode in Space Plasmas," Frontiers in Physics **8**, 1–14 (2020).

[44] I. Bernstein, "Waves in a Plasma in a Magnetic Field," Physical Review **109** (1958).

[45] D. Verscharen and B. D. G. Chandran, "NHDS: The New Hampshire Dispersion Relation Solver," Research Notes of the AAS **2**, 13 (2018), arXiv:1804.10096.

[46] F. Sahraoui, M. L. Goldstein, G. Belmont, P. Canu, and L. Rezeau, "Three dimensional anisotropic k spectra of turbulence at subproton scales in the solar wind," Physical Review Letters **105**, 1–4 (2010).

[47] Y. Narita, S. Gary, S. Saito, K.-H. Glassmeier, and U. Motschmann, "Dispersion relation analysis of solar wind turbulence," Geophysical Research Letters **38**, 2–5 (2011).

[48] O. W. Roberts, X. Li, and B. Li, "Kinetic Plasma Turbulence in the Fast Solar Wind Measured By Cluster," The Astrophysical Journal **769** (2013), 10.1088/0004-637X/769/1/58.

[49] Y. Narita, "Four-dimensional energy spectrum for space-time structure of plasma turbulence," Nonlinear Processes in Geophysics **21**, 41–47 (2014).

[50] S. Bourouaine, O. Alexandrova, E. Marsch, and M. Maksimovic, "On Spectral Breaks in the Power Spectra of Magnetic Fluctuations in Fast Solar Wind Between 0.3 and 0.9 Au," The Astrophysical Journal **749**, 102 (2012).

[51] S. P. Gary, "Low-frequency waves on a high-beta collisionless plasma: Polarization, compressibility and helicity," Journal of Plasma Physics **35**, 431–447 (1986).

[52] Y. Narita, E. Marsch, C. Perschke, K.-H. Glassmeier, U. Motschmann, and H. Comişel, "Wave–particle resonance condition test for ion-kinetic waves in the solar wind," Annales Geophysicae **34**, 393–398 (2016).

[53] Y. Narita, E. Marsch, C. Perschke, U. Motschmann, K. H. Glassmeier, and H. Comisel, "Corrigendum to "Wave–particle resonance condition test for ion-kinetic waves in the solar wind" published in Ann. Geophys., 34, 393–398, 2016," Annales Geophysicae **34** (2016), 10.5194/angeo-34-393-2016-corrigendum.

[54] S. Gary, *Theory of Space Plasma Microinstabilities* (Cambridge University Press, 1993).

[55] F. Sahraoui, S. Y. Huang, G. Belmont, M. L. Goldstein, A. Rétino, P. Robert, and J. De Patoul, "SCALING OF THE ELECTRON DISSIPATION RANGE OF SOLAR WIND TURBULENCE," The Astrophysical Journal **777**, 15 (2013).

[56] O. W. Roberts, O. Alexandrova, P. Kajdič, L. Turc, D. Perrone, C. P. Escoubet, and A. Walsh, "Variability of the Magnetic Field Power Spectrum in the Solar Wind at Electron Scales," The Astrophysical Journal **850**, 120 (2017).

[57] G. Howes, J. TenBarge, W. Dorland, E. Quataert, A. Schekochihin, R. Numata, and T. Tatsuno, "Gyrokinetic Simulations of Solar Wind Turbulence from Ion to Electron Scales," Physical Review Letters **107**, 035004 (2011).

[58] S. Zenitani, M. Hesse, A. Klimas, and M. Kuznetsova, "New Measure of the Dissipation Region in Collisionless Magnetic Reconnection," Physical Review Letters **106**, 195003 (2011), arXiv:1104.3846.

[59] S. D. Bale, P. J. Kellogg, F. S. Mozer, T. S. Horbury, and H. Reme, "Measurement of the Electric Fluctuation Spectrum of Magnetohydrodynamic Turbulence," Physical Review Letters **94**, 215002 (2005).

[60] C. H. K. Chen, A. Mallet, T. A. Yousef, A. Schekochihin, and T. Horbury, "Anisotropy of Alfvénic turbulence in the solar wind and numerical simulations," Monthly Notices of the Royal Astronomical Society **415**, 3219–3226 (2011).

[61] G. G. Howes, S. C. Cowley, W. Dorland, G. W. Hammett, E. Quataert, and A. A. Schekochihin, "A model of turbulence in magnetized plasmas: Implications for the dissipation range in the solar wind," Journal of Geophysical Research: Space Physics **113**, 1–24 (2008).

[62] R. Bandyopadhyay, L. Sorriso-Valvo, A. Chasapis, P. Hellinger, W. H. Matthaeus, A. Verdini, S. Landi, L. Franci, L. Matteini, B. L. Giles, D. J. Gershman, T. E. Moore, C. J. Pollock, C. T. Russell, R. J. Strangeway, R. B. Torbert, and J. L. Burch, "In Situ Observation of Hall Magnetohydrodynamic Cascade in Space Plasma," Physical Review Letters **124**, 225101 (2020), arXiv:1907.06802.

[63] W. H. Matthaeus, "Turbulence in space plasmas: Who needs it?" Physics of Plasmas **28** (2021), 10.1063/5.0041540.

[64] J. He, D. Duan, T. Wang, X. Zhu, W. Li, D. Verscharen, X. Wang, C. Tu, Y. Khotyaintsev, G. Le, and J. Burch, "Direct Measurement of the Dissipation Rate Spectrum around Ion Kinetic Scales in Space Plasma Turbulence," The Astrophysical Journal **880**, 121 (2019).

[65] J. He, X. Zhu, D. Verscharen, D. Duan, J. Zhao, and T. Wang, "Spectra of Diffusion, Dispersion, and Dissipation for Kinetic Alfvénic and Compressive Turbulence: Comparison between Kinetic Theory and Measurements from MMS," The Astrophysical Journal **898**, 43 (2020).

[66] O. W. Roberts, Y. Narita, and C.-P. Escoubet, "Multi-scale analysis of compressible fluctuations in the solar wind," Annales Geophysicae **36**, 47–52 (2018).

[67] J. S. Zhao, Y. Voitenko, M. Y. Yu, J. Y. Lu, and D. J. Wu, "PROPERTIES OF SHORT-WAVELENGTH OBLIQUE ALFVEN AND SLOW WAVES," **793** (2014), 10.1088/0004-637X/793/2/107.

[68] D. Perrone, O. Alexandrova, A. Mangeney, M. Maksimovic, C. Lacombe, V. Rakoto, J. C. Kasper, and D. Jovanovic, "COMPRESSIVE COHERENT STRUCTURES AT ION SCALES IN THE SLOW SOLAR WIND," The Astrophysical Journal **826**, 196 (2016).

[69] J. Soucek and C. P. Escoubet, "Cluster observations of trapped ions interacting with magnetosheath mirror modes," Annales Geophysicae **29**, 1049–1060 (2011).

[70] S. Yao, J.-S. He, E. Marsch, C.-Y. Tu, A. Pedersen, H. Rème, and J. G. Trotignon, "Multi-Scale Anti-Correlation Between Electron Density and Magnetic Field Strength in the Solar Wind," The Astrophysical Journal **728**, 146 (2011).

[71] D. Verscharen, E. Marsch, U. Motschmann, and J. Müller, "Kinetic cascade beyond magnetohydrodynamics of solar wind turbulence in two-dimensional hybrid simulations," Physics of Plasmas **19**, 1–9 (2012), arXiv:arXiv:1201.2784v2.

[72] G. G. Howes and K. D. Nielson, "Alfvén wave collisions, the fundamental building block of plasma turbulence. I. Asymptotic solution," Physics of Plasmas **20**, 072302 (2013).

[73] Y. Narita, "Space–time structure and wavevector anisotropy in space plasma turbulence," Living Reviews in Solar Physics **15** (2018), 10.1007/s41116-017-0010-0.

[74] C. Perschke, Y. Narita, U. Motschmann, and K.-H. Glassmeier, "MULTI-SPACECRAFT OBSERVATIONS OF LINEAR MODES AND SIDEBAND WAVES IN ION-SCALE SOLAR WIND TURBULENCE," The Astrophysical Journal **793**, L25 (2014).

[75] C. Perschke, Y. Narita, U. Motschmann, and K.-H. Glassmeier, "Observational Test for a Random Sweeping Model in Solar Wind Turbulence," Physical Review Letters **116**, 1–5 (2016).

[76] Y. Nariyuki and T. Hada, "Remarks on nonlinear relation among phases and frequencies in modulational instabilities of parallel propagating Alfvén waves," Nonlinear Processes in Geophysics **13**, 425–441 (2006).

[77] G. G. Howes, "A dynamical model of plasma turbulence in the solar wind," Philosophical Transactions of the Royal Society A: Mathematical, Physical and Engineering Sciences **373** (2015), 10.1098/rsta.2014.0145, arXiv:1502.04109.

[78] A. F. Viñas and M. L. Goldstein, "Parametric instabilities of circularly polarized large-amplitude dispersive Alfvén waves: excitation of parallel-propagating electromagnetic daughter waves," Journal of Plasma Physics **46**, 107–127 (1991).

[79] J. Zhao, Y. Voitenko, D. J. Wu, and J. De Keyser, "Nonlinear Generation of Kinetic-scale Waves by Magnetohydrodynamic Alfvén Waves and Nonlocal Spectral Transport in the Solar Wind," The Astrophysical Journal **785** (2014).

[80]D. Verscharen, E. Marsch, U. Motschmann, and J. Müller, "Parametric decay of oblique Alfvén waves in two-dimensional hybrid simulations," Physical Review E **86**, 027401 (2012).
[81]H. Comişel, Y. Narita, and U. Motschmann, "Multi-channel coupling of decay instability in three-dimensional low-beta plasma," Annales Geophysicae **37**, 835–842 (2019).
[82]T. G. Jenkins, T. M. Austin, D. N. Smithe, J. Loverich, and A. H. Hakim, "Time-domain simulation of nonlinear radiofrequency phenomena," Physics of Plasmas **20**, 012116 (2013).
[83]J. M. TenBarge and G. G. Howes, "CURRENT SHEETS AND COLLISIONLESS DAMPING IN KINETIC PLASMA TURBULENCE," The Astrophysical Journal **771**, L27 (2013).
[84]F. Sahraoui, L. Hadid, and S. Huang, *Reviews of Modern Plasma Physics*, Vol. 4 (Springer Singapore, 2020) pp. 1–33.
[85]K. G. Klein, O. Alexandrova, J. Bookbinder, D. Caprioli, A. W. Case, B. D. G. Chandran, L. J. Chen, T. Horbury, L. Jian, J. C. Kasper, O. L. Contel, B. A. Maruca, W. Matthaeus, A. Retino, O. Roberts, A. Schekochihin, R. Skoug, C. Smith, J. Steinberg, H. Spence, B. Vasquez, J. M. TenBarge, D. Verscharen, and P. Whittlesey, "[Plasma 2020 Decadal] Multipoint Measurements of the Solar Wind: A Proposed Advance for Studying Magnetized Turbulence," (2019), arXiv:1903.05740, arXiv:1903.05740.
[86]L. Dai, C. Wang, Z. Cai, W. Gonzalez, M. Hesse, P. Escoubet, T. Phan, V. Vasyliunas, Q. Lu, L. Li, L. Kong, M. Dunlop, R. Nakamura, J. He, H. Fu, M. Zhou, S. Huang, R. Wang, Y. Khotyaintsev, D. Graham, A. Retino, L. Zelenyi, E. E. Grigorenko, A. Runov, V. Angelopoulos, L. Kepko, K. J. Hwang, and Y. Zhang, "AME: A Cross-Scale Constellation of CubeSats to Explore Magnetic Reconnection in the Solar–Terrestrial Relation," Frontiers in Physics **8**, 1–14 (2020).
[87]MMS Team, "MMS Science Data Centre," `https://lasp.colorado.edu/mms/sdc/public/`, (2021).

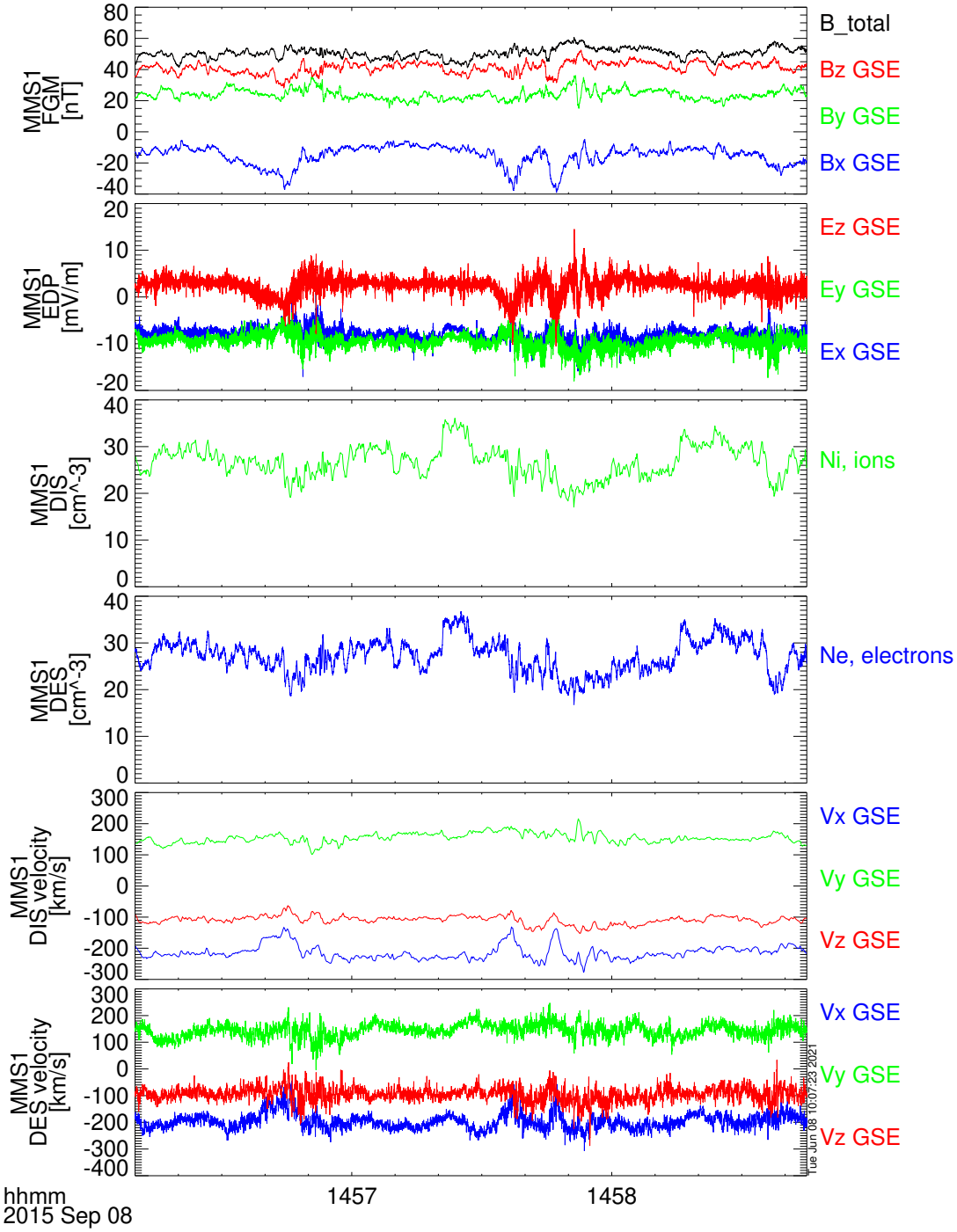

FIG. 1. Measured data from the MMS1 spacecraft. From top to bottom, the magnetic field from the fluxgate magnetometer, the electric field in the spacecraft frame from the spin plane double probes and the axial double probes, the ion density, the electron density, the ion velocity, and the electron velocity from the fast plasma investigation.

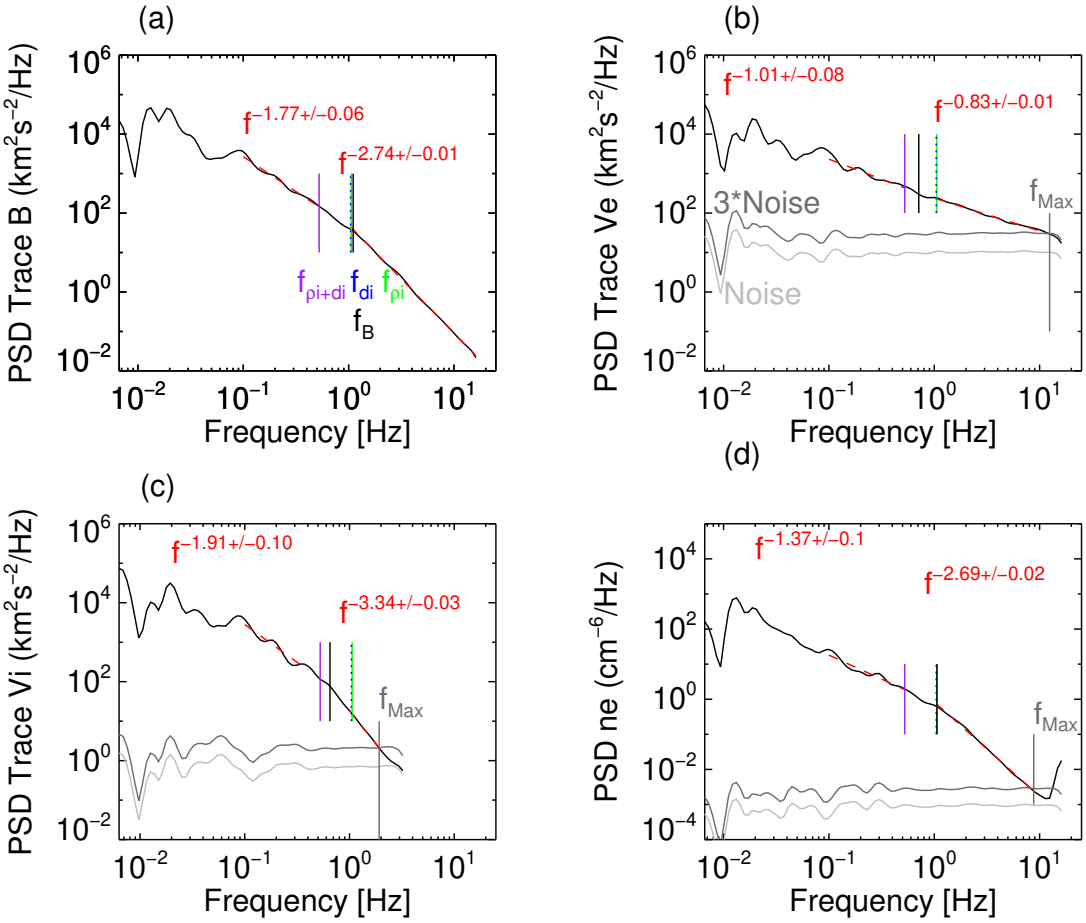

FIG. 2. Wavelet power spectrum of the trace magnetic field spectrum (a) the trace electron velocity spectrum (b), the trace ion velocity spectra (c), and the electron density spectrum (d). The vertical lines denote different ion scales, with purple denoting the combined scale, green denoting the ion inertial, and blue denoting the ion gyro scale. The black vertical lines denotes the intersection of the power-law fits between large and small scales. The grey curve denotes the estimated noise floor based on the statistical uncertainties[26], and the dark grey curve denotes three times the noise floor, which is used to find the maximum reliable frequency.

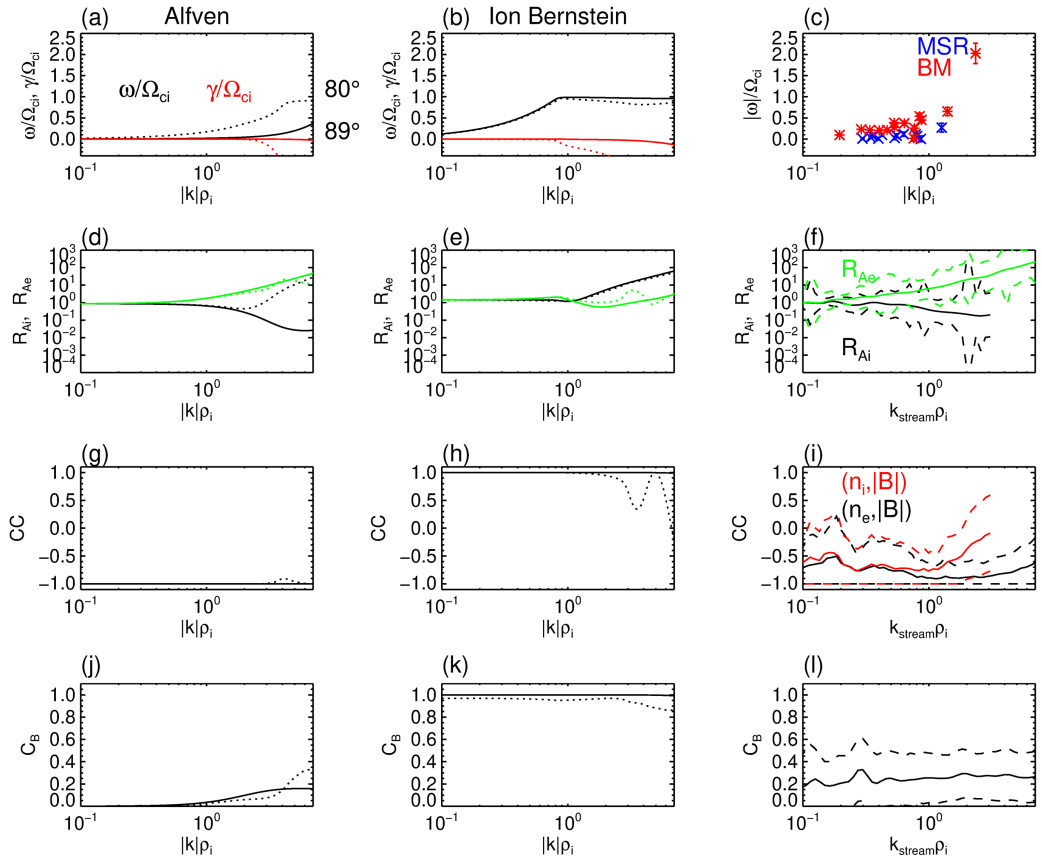

FIG. 3. The first two columns show the predictions of linear theory for a Kinetic Alfvén wave (column 1) and for an ion Bernstein wave (column 2). Panels (a,b) show the frequency, with the real part in black and the imaginary part in red. Solid lines denote a propagation angle of 89° and dashed lines denote an angle of 80°. Panels (d,e) show the ion Alfvén ratio in black and the electron Alfvén ratio in green. Panels (g,h) show the cross correlation of density and compressive magnetic field. Panels (j,k) show the magnetic compressibility. Column 3 shows the observations from the MMS spacecraft. Panel (c) shows the dispersion relation diagram from the MMS data using the MSR data (blue) and Bellan method (red). Panel (f) shows the measured ion and electron Alfvén ratios (solid lines) and their relative errors (for display on logarithimc axis). Panel (i) shows the cross correlation of the density and magnetic field strength (solid lines), dashed lines denote the standard deviations. Panel (l) shows the compressibility (solid lines) and the standard deviations.

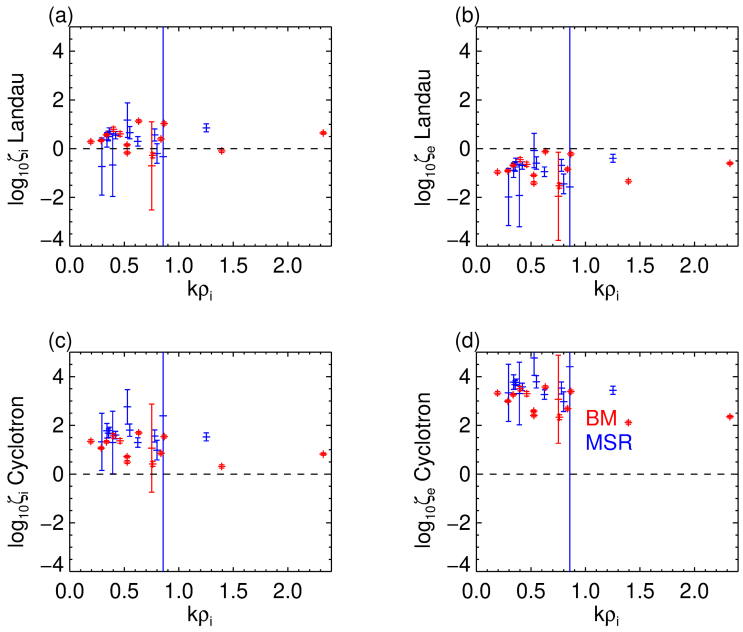

FIG. 4. The resonance parameters as a function of wavenumber for the ion Landau resonance (a) the electron Landau resonance (b) the first ion cyclotron resonance (c) and the first electron cyclotron resonance (d). The error bars denote the relative error based on the propagation of the error on the plasma frame frequency.

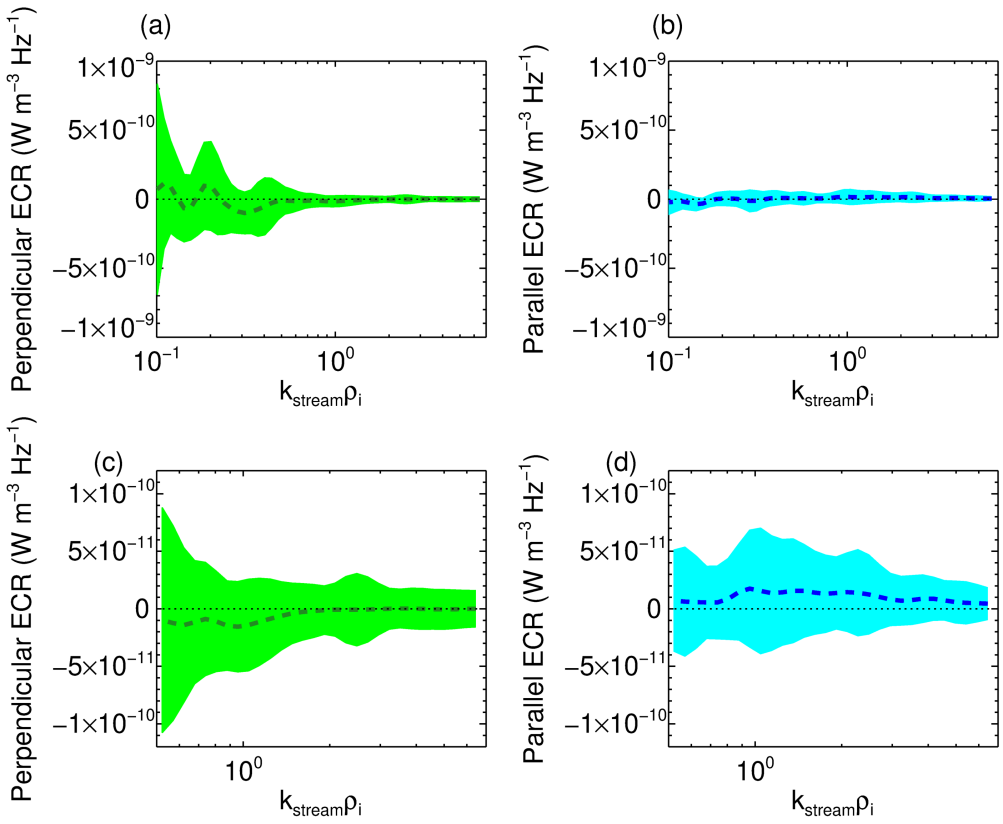

FIG. 5. Scale dependent energy conversion rate defined in Eq. 7 for the perpendicular components (a,c) and the parallel components (b,d)